EDGE ARTICLE

Check for updates

Borinostats: solid-phase synthesis of carborane-capped histone deacetylase inhibitors with a tailor-made selectivity profile†

Christoph Selg,[a] Andrea Schöler,[a] Julian Schliehe-Diecks,[b] Maria Hanl,[c] Laura Sinatra,[a] Arndt Borkhardt,[b] Menyhárt B. Sárosi, [iD][d] Sanil Bhatia,[b] Evamarie Hey-Hawkins [iD][d] and Finn K. Hansen [iD] *[c]

The elevated expression of histone deacetylases (HDACs) in various tumor types renders their inhibition an attractive strategy for epigenetic therapeutics. One key issue in the development of improved HDAC inhibitors (HDACis) is the selectivity for single HDAC isoforms over unspecific pan inhibition to minimize off-target toxicity. Utilizing the carborane moiety as a fine-tuning pharmacophore, we herein present a robust solid phase synthetic approach towards tailor-made HDACis meeting both ends of the selectivity spectrum, namely pan inhibition and highly selective HDAC6 inhibition.

Introduction

Histone deacetylases (HDACs) and their counterpart, the histone acetyl transferases (HATs), comprise two families of enzymes that play a key-role in the regulation of numerous genes and proteins.[1,2] By controlling the reversible acetylation status of the ε-amino groups of lysine residues at the N-terminal domain of histone and non-histone proteins, they regulate the state of condensation of the DNA without impinging the DNA sequence itself:[3] while HATs will cause chromatin structure to stretch into euchromatin and thus provide access to the DNA for the specific enzyme or other protein complexes involved in transcription and repair, HDACs induce condensed and transcriptionally inactive heterochromatin.[1,2,4] As overexpression of HDACs was shown to be linked with several cancer types, their selective inhibition results in several anticancer effects including terminal differentiation, growth arrest and apoptosis in cancer cells.[4–7] Therefore, HDAC inhibitors (HDACis) have emerged as valuable epigenetic modulators for treatment of cancer[6–8] as well as HIV,[9] inflammatory diseases,[10] immune disorders, neurodegenerative[11–13] and parasitic diseases.[15] There are eighteen human HDAC isoforms that have been divided into four classes according to their primary homology to yeast: class I (HDACs 1, 2, 3 and 8), class IIa (HDACs 4, 5, 7, 9), class IIb (HDACs 6 and 10), class III (human sirtuins 1–7) and class IV (HDAC11).[24] Within the HDAC family, HDAC6 has drawn major research attention due to occupying a very unique space in the therapeutic spectrum covering intracellular transport, neurotransmitter release, and aggresome formation.[13,16] Primarily localized in the cytoplasm it regulates the acetylation of α-tubulin, HSP90,[17,18] tau, cortactin, and amyloid β, and influences the microtubule formation and thereby the cell motility and metastatic potential.[19] Thus, several research groups have developed small molecule inhibitors with selectivity for this specific isoform mainly following a certain pharmacophore model (Fig. 1).

[a]*Institute for Drug Discovery, Medical Faculty, Leipzig University, Brüderstraße 34, 04103 Leipzig, Germany*

[b]*Department of Pediatric Oncology, Hematology and Clinical Immunology, Medical Faculty, Heinrich-Heine University Düsseldorf, Düsseldorf, Germany*

[c]*Pharmaceutical Institute, Department of Pharmaceutical and Cell Biological Chemistry, University of Bonn, An der Immenburg 4, 53121 Bonn, Germany. E-mail: finn.hansen@uni-bonn.de*

[d]*Institute of Inorganic Chemistry, Faculty of Chemistry and Mineralogy, Leipzig University, Johannisallee 29, 04103 Leipzig, Germany*

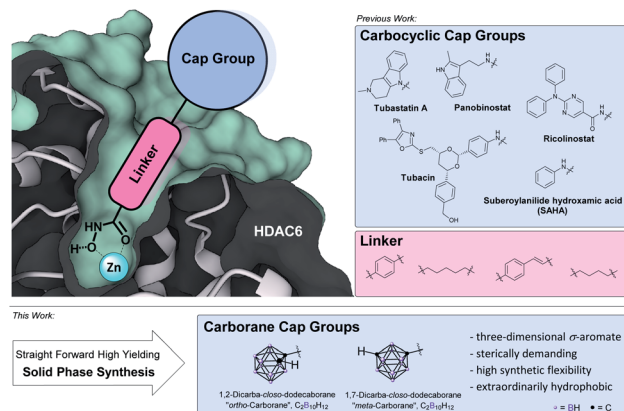† Electronic supplementary information (ESI) available. See DOI: 10.1039/d1sc02268g

Fig. 1 Pharmacophore model of selective HDACis: zinc-binding group (ZBG), hydrophobic alkyl or aryl linker and a sterically demanding, hydrophobic cap group.[48,56]

Except for class III HDACs, which are NAD⁺-dependent, all HDACs are Zn^{2+}-dependent enzymes.[20] Thus, the respective inhibitor usually possesses a zinc-binding group (ZBG), a hydrophobic linker and a cap group (Fig. 1, top left). Starting from the rather unselective FDA-approved hydroxamate-based drugs vorinostat, belinostat and panobinostat,[20] within this pharmacophore model, HDAC6 isoform selectivity was shown to be connected to steric bulk and hydrophobicity of the cap group owing to the increased size of the outer channel opening of HDAC6 with 17 Å compared to 12 Å in HDAC1.[17,21–23] High selectivity was achieved with cap groups bearing extended aromatic residues as in tubacin and tubastatin A as well as bulky cap groups as realized in ricolinostat-type HDACis.[14,22,23] In order to increase selectivity, numerous hydrophobic (hetero)aromatic and, to some extent aliphatic cap groups were described in the literature.[20,21] These carbon-based systems are for the most part limited to a two-dimensional shape as larger carbocyclic skeletons like adamantyl-, norbornenyl-, bicyclo-[2.2.2]octanyl- or fullerenyl-residues pose problems due to limited modification sites and possible rearrangement reactions or their sheer size.[25] Therefore, when it comes to hydrophobic, sterically demanding scaffolds, an emerging building block in drug design is the carborane moiety.[26] Replacement of (hetero)aryl moieties by these extremely versatile boron clusters has been widely applied and often resulted in dramatically increased potency, target selectivity and lower toxicity.[25,27] Furthermore, carboranes play a key role in the development of boron neutron capture therapy (BNCT) agents and as carriers in nanomedicinal applications.[29,30] Carboranes are a family of polyhedral clusters comprised of CH and BH vertices with the icosahedral closo-dicarbadodecaborane ($C_2B_{10}H_{12}$) being the most prominent and well-examined member.[27,28] For symmetrical reasons, the two carbon atoms can be arranged within the icosahedron separated by one (ortho-/1,2-), two (meta-/1,7-) or three (para-carborane/closo-1,12-dicarbadodecaborane) bonds (Fig. 1, bottom). The size of the cluster is in between a rotating phenyl ring and adamantane. The cluster fragments CH and BH are interconnected by a strong network of multi-electron-multi-center bonds and thus represent a completely delocalized three-dimensional σ-aromatic compound (deemed "superaromatic") of very high stability.[31] Bearing acidic (carbon-centered) and hydridic (boron-centered) hydrogen atoms, carboranes exhibit a peculiar interaction profile where besides the classic hydrophobic interactions, also hydrogen bonds C–H···X (X = O, N, S, F, π-system) and the so-called dihydrogen bonds B–H···H–X (with $\chi_X > \chi_H > \chi_B$) are formed.[32,33] As opposed to carbon cage structures, for carboranes manifold achiral, chiral and chiral-at-cage modifications at carbon- as well as at boron-vertices are described in the literature, thus paving the way also for the evaluation and design of target-specific asymmetric drugs.[34,35]

While boron-containing drugs like bortezomib, crisaborole and tavaborole are established therapeutics, carborane drugs are still scarce in clinical trials.[30,36–38] Within this branch, a limited number of boron-containing HDACis have been investigated.[39,40] However, only one of them was carborane-based and to the best of our knowledge none of them were tested for their HDAC6 selectivity. In the present publication we

therefore seek to establish a systematic approach to carborane-based HDACis to provide a solid foundation for further investigations. By synthesizing a small compound library, we want to enable the direct head-to-head comparison of different carborane cap groups employing a set of known and successfully employed linker groups in combination with the well-investigated aryl or alkyl hydroxamate zinc-binding group. The hit compounds will be further compared to their respective phenyl analogues.

Results and discussion

Despite the readily synthetic availability of aniline-type carborane derivatives we chose the electrophilic carboxylic acid for the formation of the amide connectivity,[41] as carboranes with directly bonded electron-withdrawing substituents are prone to degradation by base. Cluster deboronation can also occur in biological environments. Furthermore, as the clusters impose a strong electron-withdrawing effect on the adjacent nitrogen, carboranyl amines exhibit extreme low nucleophilicity.[42] To provide different degrees of freedom in movement we decided to evaluate the carborane analogues of phenylacetic acid and benzoic acid (Scheme 1).

Following the synthetic protocol of Nekvinda and co-workers,[43] closo-1,2-dicarbadodecaborane (ortho-1) was mono-lithiated and treated with oxirane to afford hydroxymethyl carborane 2 which was subsequently oxidized with CrO_3 to form the desired carboxymethyl carborane 3. As benzoic acid analogues of ortho-carborane prove problematic in amide couplings, we chose the meta isomer, closo-1,7-dicarbadodecaborane (meta-1), for our second cap group scaffold.[44] The respective carboxylic acid 4 was obtained following a slightly modified literature procedure of Kasar and co-workers.[46] Monolithiation of meta-1 and subsequent treatment with gaseous CO_2 afforded 4 in quantitative yield (Scheme 1).

With the carborane cap group precursors 3 and 4 in hand, an elaborate synthetic approach for the linker and hydroxamate moieties was developed. To overcome the problems of the aforementioned possible deboronation that might occur under strongly basic conditions associated with the typical synthesis of hydroxamic acids through hydroxylaminolysis,[40] we envisioned that a solid-phase synthesis as recently described by our
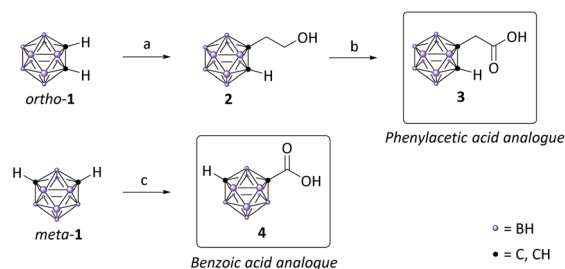
Scheme 1 Synthesis of the carborane building blocks. Reagents: (a) (i) n-BuLi, hexane, 0 °C; (ii) C_2H_4O, 0 °C; (iii) AcOH, MeOH, rt, 45%; (b) CrO_3, acetone, AcOH, H_2O, rt, 69%; c) (i) n-BuLi, Et_2O, −78 °C; (ii) $CO_{2(g)}$, −78 °C; (iii) H_2O, rt, quant.
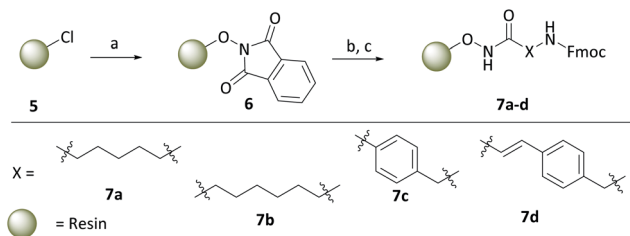
Scheme 2 Synthesis of the modified resins **7a–d** with four different linkers. Reagents: (a) PhthN–OH, NEt$_3$, DMF, 24 h, rt; (b) N$_2$H$_4$·H$_2$O, MeOH, 30 min, rt; (c) Fmoc–linker–COOH, HATU, HOBt·H$_2$O, DIPEA, DMF, 18 h, rt.

group would be the suitable tool.[47] Beside the prevention of harsh basic conditions, this methodology could offer a fast and efficient carborane-based HDACi library expansion through a parallel synthesis approach. Consequently, we treated in a first step the commercially available 2-chlorotritylchloride resin **5** with *N*-hydroxyphthalimide to form the modified resin **6**. The phthaloyl residue in turn is cleaved using a 5% methanolic hydrazine solution to obtain a free hydroxylamine which can be coupled in a HATU-mediated amide coupling with an *N*-Fmoc protected linker to form the modified resins **7a–d** (Scheme 2).

To cover a broad spectrum of possible HDACis, we chose linker moieties that were already employed in unselective and selective HDACis described in the literature in resemblance to ricolinostat, vorinostat and tubacin, two different chain lengths, namely C$_5$ and C$_6$ alkyl linkers (**7a**, **7b**), as well as a tubastatin-type benzyl (**7c**) and a panobinostat-type vinyl-benzyl linker (**7d**) were selected (Scheme 2).

After Fmoc deprotection of the modified resins **7a–d**, amide coupling with the respective carboranyl carboxylic acid cap groups **3** and **4** and subsequent cleavage with TFA afforded the desired carborane-capped hydroxamates **8a–d** and **9a–d** in very good yields (Scheme 3).

While coupling of *ortho*-carborane derivative **3** was achieved flawlessly under standard conditions using HATU, DIPEA and DMF, the *meta*-carboranyl carboxylic acid **4** could only be coupled in moderate yields. However, following the procedure described by Scholz *et al.*, by the replacement of HATU with the more active COMU, excellent yields were also achieved with the sterically demanding and less reactive **4**.[44b]
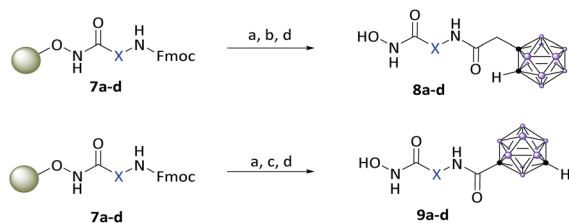
Scheme 3 Fmoc deprotection of the modified resins **7a–d**, amide coupling with the carboranyl cap groups and cleavage off the resin. Reagents: (a) 20% piperidine in DMF, rt; (b) **3**, HATU, DIPEA, DMF, 18 h, rt, (c) **4**, COMU, DIPEA, DMF, 18 h, rt; (d) 5% TFA, DCM, 1 h, rt, 74–99%. For definition of X see Scheme 2.

With the eight hydroxamates **8a–d** and **9a–d** in hand, we set out to explore their inhibitory activity against HDAC1 and HDAC6 in a fluorogenic assay using ZMAL (*Z*-Lys(Ac)-AMC) as substrate and vorinostat (suberoylanilide hydroxamic acid, **SAHA**) as a control (Table 1) following our previously published protocol.[45] To our delight, all new compounds showed IC$_{50}$ values for HDAC6 in the double- or even single-digit nanomolar range comparable to those of **SAHA** (IC$_{50}$: 0.031 μM). Two of the compounds (**9a** and **9d**) showed improved HDAC6 inhibition compared to the control. Compound **9d** was identified as the most potent HDAC6 inhibitor (IC$_{50}$: 0.006 μM).

Due to a relatively even distribution of IC$_{50}$ values no clear structure–activity relationship could be assigned for HDAC6 inhibition. For the activity against HDAC1, however, a clear selectivity trend was observed (Fig. 2).

Three of the compounds bearing an alkyl chain linker (**8a**, **9a** and **9b**) showed moderate (12- to 18-fold) preference for HDAC6 with slightly better inhibitory activity for the longer chains. The results of the short chain derivative **8b** (SF$^{6/1}$: 2) whose net chain length and carbonyl group positions match the parent aryl analogue pan inhibitor **SAHA** (SF$^{6/1}$: 3) showed no clear preference.
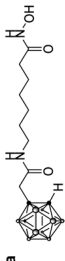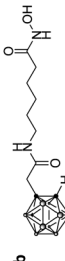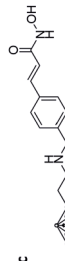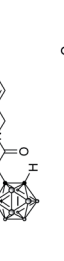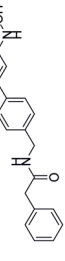
Also, for the vinylbenzyl hydroxamates **8c** and **9c**, inhibition of both HDACs was very similar. Notably, inverse preference was observed between the two carborane cap groups shifting from either two-fold HDAC1 preference for **8c** to two-fold HDAC6 preference for **9c**. In contrast to this unselective inhibitory activity, the tubastatin A analogues with a benzyl linker (**8d** and **9d**) showed excellent selectivity for HDAC6 whilst also maintaining very high inhibitory activity. Thus, we identified the *meta*-carboranyl hydroxamate **9d** as the hit compound with an IC$_{50}$ value of 0.006 μM and a more than 280-fold selectivity for HDAC6 (Table 1 and Fig. 2).

To investigate the influence of the carborane moiety, we synthesized aryl analogues for the best pan inhibitory compound **8c** and the best selective HDAC6 inhibitor **9d**. The synthesis was carried out employing our solid-phase protocol to afford vinylbenzyl derivative **10** from phenylacetic acid and benzyl derivative **11** using benzoic acid. Both phenyl analogues **10** and **11** showed good inhibitory activity against HDAC6 with IC$_{50}$ values of 0.095 μM and 0.025 μM, respectively (Table 1). The HDAC6 selectivity (SF$^{6/1}$: 2 and 29 resp.) was distributed the same way as observed for parent compounds **8c** and **9d**, yet the carborane compounds clearly outperformed their corresponding phenyl analogue in terms of HDAC6 inhibition and, in the case of **9d**, selectivity.

To evaluate the anticancer properties of the carborane-capped HDACis, compounds **8a–d** and **9a–d**, as well as their phenyl analogues **10** and **11** were tested in MTT assays in the ovarian cancer cell line A2780, again using the FDA-approved HDACi vorinostat (**SAHA**) as positive control.[45] The results are summarized in Table 1. All compounds demonstrated anti-proliferative effects in the single-digit micromolar concentration range. The most potent carborane-capped HDACi was compound **8c** with an IC$_{50}$ value of 1.66 μM.

Encouraged by these promising results, we performed additional HDAC isoform profilings examining the HDAC6

Table 1 *In vitro* target inhibition of HDAC1 and HDAC6 with selectivity factor $SF^{6/1}$ for HDAC6 over HDAC1 and antiproliferative activity (MTT assay) against the human ovarian cancer cell line A2780

Structure	Target inhibition IC_{50} [a] [μM]		MTT IC_{50} [b] [μM]	
	HDAC1	HDAC6	$SF^{6/1}$	A2780
8a	0.451 ± 0.023	0.037 ± 0.006	12	5.78 ± 1.68
8b	0.101 ± 0.003	0.045 ± 0.011	2	4.64 ± 0.95
8c	**0.015 ± 0.002**	**0.031 ± 0.004**	**0.5**	**1.66 ± 0.81**
8d	2.888 ± 0.049	0.059 ± 0.007	49	4.85 ± 1.64
10	0.176 ± 0.007	0.095 ± 0.008	2	1.39 ± 0.30
SAHA	0.094 ± 0.014	0.031 ± 0.009	3	1.03 ± 0.27

Structure	Target inhibition IC_{50} [a] [μM]		MTT IC_{50} [b] [μM]	
	HDAC1	HDAC6	$SF^{6/1}$	A2780
9a	0.440 ± 0.166	0.024 ± 0.005	18	3.98 ± 0.95
9b	1.328 ± 0.039	0.078 ± 0.0003	17	5.28 ± 1.25
9c	0.081 ± 0.014	0.040 ± 0.008	2	3.07 ± 1.41
9d	**1.715 ± 0.002**	**0.006 ± 0.0001**	**286**	**4.60 ± 1.67**
11	0.725 ± 0.041	0.025 ± 0.002	29	5.04 ± 1.21

[a] Assays carried out with $n \geq 2$ (each in duplicate wells), values are shown as means ± SD. [b] Assays carried out with $n \geq 3$ (each in duplicate wells), values are shown as means ± SD.
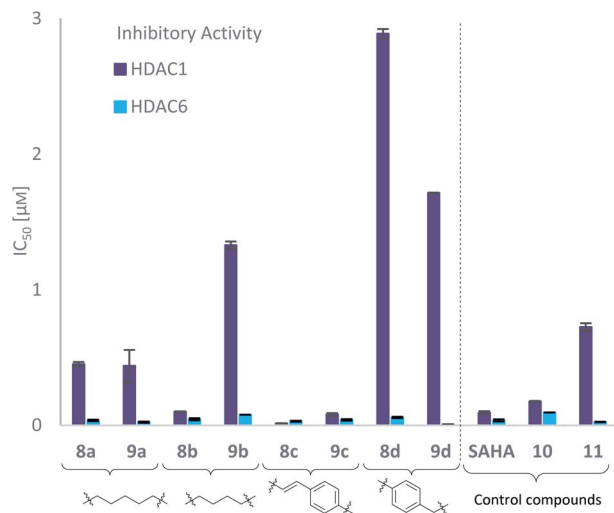
Fig. 2 Target inhibition indicated by IC$_{50}$ values (μM) of carborane-based hydroxamates **8a–d**, **9a–d** and control compounds **SAHA**, **10** and **11** grouped by linker against HDAC1 and HDAC6, determined by fluorogenic HDAC inhibition assays.

selectivity of the two most potent compounds **8c** and **9d** over all class I isoforms with **SAHA** as control and in the case of HDAC8, also panobinostat (Table 2).

Considering HDAC2 and HDAC3, again, **8c** showed non-selective behavior while compound **9d** exhibited substantial

selectivity for HDAC6 over HDAC2 and HDAC3 (309- and 224-fold, respectively). The IC$_{50}$ values for HDAC8 were greater than 1 μM and indicated neglectable inhibition for both compounds.

As already observed for tubastatin A and panobinostat, the potent HDAC6 inhibition may be the result of π–π stacking interactions between the linker aryl groups and the adjacent phenylalanine residues inside the hydrophobic channel.[48,54] To further undermine this assumption, compounds **8c** and **9d** were docked into the human HDAC6 catalytic domain 2 (hHDAC6-CD2, Fig. 3A and B). Hydroxamate inhibitors are known to coordinate to the HDAC Zn^{2+} ion through mono- or bidentate binding modes.[48,54,55] A monodentate Zn^{2+}-binding was predicted for **8c** and the amido NH group forms a hydrogen bond with S568. The phenyl ring of **8c** forms a π–π stacking interaction with F680. On the other hand, a bidentate Zn^{2+}-binding was predicted for **9d**. The phenyl ring of **9d** forms a π–π stacking interaction with F620 and the amido CO group can potentially form a hydrogen bond with S568.

The carborane clusters of both compounds form dihydrogen bonds with H500 and P501, but the *ortho*-carborane of **8c** additionally interacts with F620. The dihydrogen bonds between the ligands and key hHDAC6-CD2 residues H500 and P501 certainly contribute to the observed potent inhibition of HDAC6. The sterically demanding hydrophobic carborane cap groups point outwards the hydrophobic channel and align to HDACs surface binding domain which leaves sufficient space for the carborane to act as isoform selection parameter without decreasing target inhibition.

Table 2 *In vitro* target inhibition of HDAC6 (class IIb) and class I isoforms HDAC1, HDAC2, HDAC3, and HDAC8

| Compound | Target inhibition IC$_{50}$ [μM][a] | | | | |
	HDAC1[b]	HDAC2[b]	HDAC3[b]	HDAC6[b]	HDAC8[c]
8c	0.015 ± 0.002	0.020 ± 0.004	0.021 ± 0.001	0.031 ± 0.004	1.661 ± 0.126
9d	1.715 ± 0.002	1.857 ± 0.167	1.346 ± 0.003	0.006 ± 0.0001	5.780 ± 0.192
SAHA	0.094 ± 0.014	0.163 ± 0.015	0.113 ± 0.004	0.031 ± 0.009	3.410 ± 0.494
Panobinostat	n.d.	n.d.	n.d.	n.d.	0.166 ± 0.015

[a] Assays carried out with $n \geq 2$ (each in duplicate wells), values are shown as means ± SD. [b] Z-Lys(Ac)-AMC was used as substrate. [c] Boc-Lys-(Tfa)-AMC was used as substrate. n.d.: not determined.
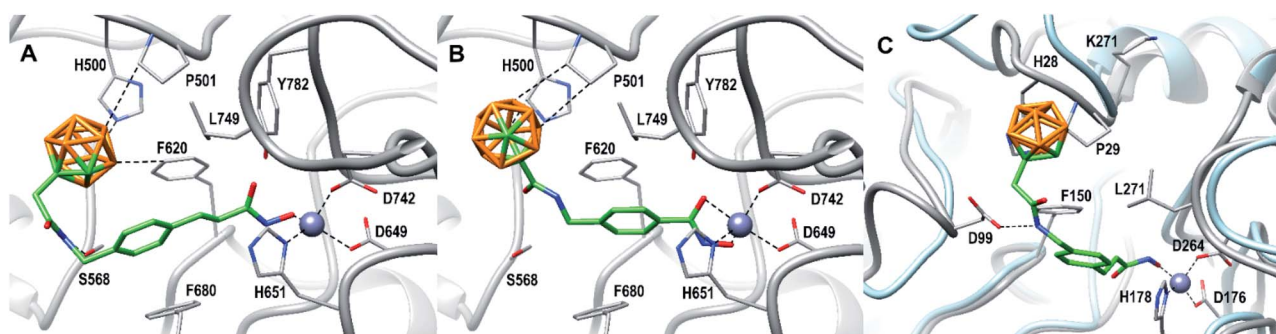
Fig. 3 **8c** (A) and **9d** (B) docked into the human HDAC6 catalytic domain 2 (PDB ID: 5EDU).[48] HDAC6 is shown in gray. Residue numbering according to PDB ID: 5EDU. **8c** (C) docked into human HDAC1 (PDB ID: 5ICN).[49] HDAC1 is shown in grey. Residue numbering according to PDB ID: 5ICN. Superimposed HDAC6 backbone trace is shown in light blue for comparison (PDB ID: 5EDU). B: orange, C: gray/green, N: blue, O: red, Zn: purple. Hydrogen atoms are omitted. Ligand–receptor interaction and Zn^{2+} coordination is shown as dashed lines.
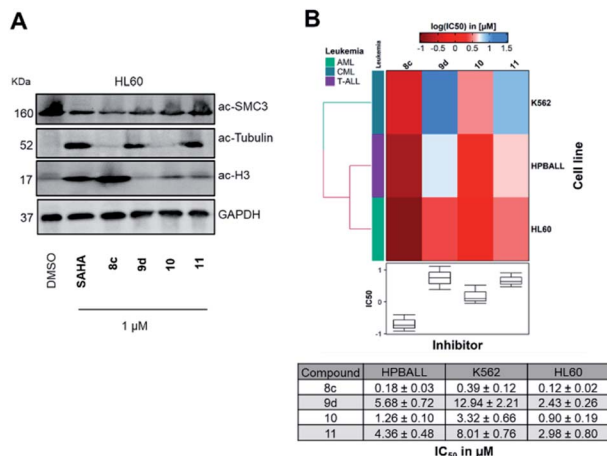
Fig. 4 (A) Immunoblotting with anti-acetyl SMC3 (HDAC8 inhibition), anti-acetyl-α-tubulin (HDAC6 inhibition) and anti-acetyl-histone H3 (HDAC1 inhibition) antibodies on HL60 cell lysates obtained after 24 h treatment at 1 μM with compounds 8c, 9d, 10, 11 or vorinostat (SAHA) as a control. (B) Comparative cellular viability (log IC_{50} μM) of three leukemic cell lines originated from different lineages (K562, HPBALL and HL60) after 72 h treatment with compounds 8c, 9d, 10 or 11. The IC_{50} data ($n = 3$) plotted as a heat map with each box of the heat map representing the mean of three independent experiments ($n = 3$), whereas the color of the individual cell is related to its position along with a log IC_{50} (μM) gradient. The table below is depicting actual IC_{50} values used for plotting these heat maps.

As an attempt to understand the different selectivity trends, 8c and 9d were docked into human HDAC1.[49] 74% of the docked poses of 8c contained a monodentate Zn^{2+}-binding. Fig. 3C shows a monodentate binding mode where the *ortho*-carborane interacts with P29 and the amido NH group forms a hydrogen bond with D99. In the case of 9d, only 39% of the docked poses chelated the zinc ion in the active site. The remaining poses of 9d did not enter the HDAC1 active site (see ESI, Fig. S1†). As a comparison, 100% of the docked HDAC6 poses for both 8c

and 9d were chelating the zinc ion. It is reasonable to assume that compound 8c exhibiting a longer linker is capable of chelating the zinc ion of both HDAC1 and HDAC6, thus inhibiting both targets, whereas the shorter benzyl linker realized in 9d in combination with a sterically demanding carborane cap is unable to efficiently engage the zinc ion in HDAC1. With the combination of our linker library and *meta*- and *ortho*-carboranes as bioisosteric phenyl mimetics, thus, we could not only significantly improve the potency, but, in the case of 9d also the selectivity of the HDACis compared to their parent phenyl analogues.

In the next step, we investigated the selectivity profile of 8c and 9d in a cellular environment using the corresponding phenyl analogues 10 and 11 as well as vorinostat (SAHA) as control compounds. The acute myeloid leukemia (AML) cell line HL60 was treated for 24 h with 1 μM of each compound and the cell lysates were subsequently immunoblotted with antibodies against acetyl-histone H3 (a marker of HDAC1-3 inhibition), acetyl-α-tubulin (a marker of HDAC6 inhibition), and acetyl-SMC3 (a marker of HDAC8 inhibition). The results are presented in Fig. 4A. None of the compounds induced acetylation of SMC3. The unselective inhibitor 8c caused hyperacetylation of histone H3 indicating inhibition of HDAC1, 2 and/or 3. As expected, the highly selective HDAC6i 9d increased only the protein levels of acetyl-α-tubulin. Consequently, the biochemical and western blot data confirm that 9d is a selective HDAC6i both in a cell-free and cellular setting.

To elucidate the antiproliferative effects of compounds 8c and 9d against a selection of cell lines from different leukemia entities, we screened both compounds in a CellTiter Glo assay against the HPBALL (T-cell acute lymphoblastic leukemia, T-ALL), K562 (chronic myeloid leukemia, CML) and HL60 (AML) cell lines. The corresponding phenyl analogues 10 and 11 were used as controls (Fig. 4B).

Compound 9d displayed moderate antiproliferative activity with IC_{50} values ranging from 2.43 to 12.94 μM, while 8c
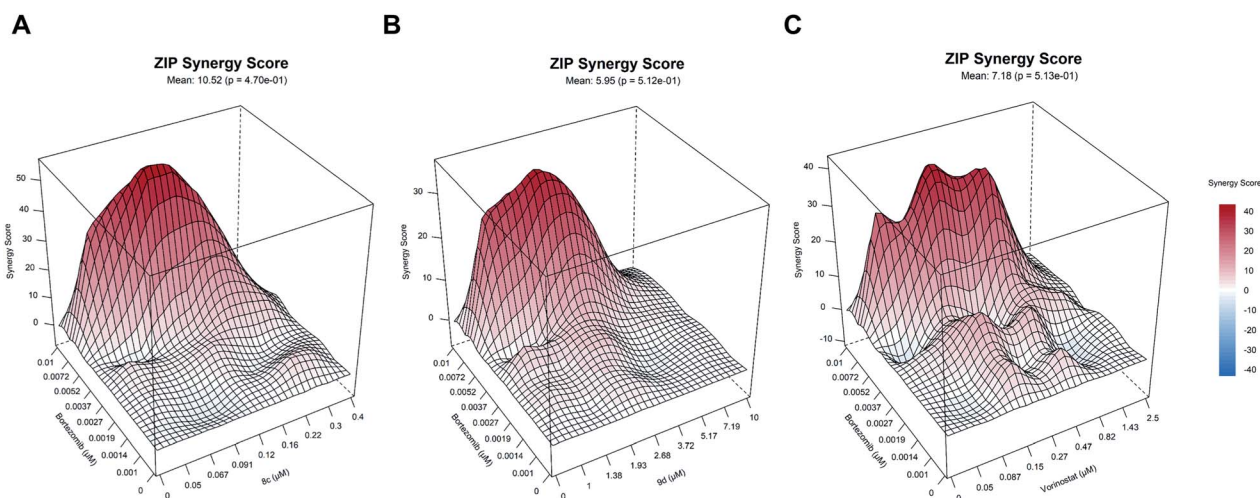

Fig. 5 (A)–(C) Illustrative synergy map of 8c, 9d and vorinostat (SAHA) after 72 h co-treatment of the acute myeloid leukemia (AML) cell line HL60 with bortezomib (proteasome inhibitor) at depicted concentrations. The mean synergy score calculations were based on the ZIP model and visualizations were performed using Synergy Finder webtool.[50]

demonstrated submicromolar activity against all three cell lines with the highest activity observed in HL60 cells (IC$_{50}$: 0.12 μM). Of note, **8c** outperformed its corresponding phenyl analogue **10** in all three cell lines and showed 7–8-fold lower IC$_{50}$ values.

The relatively low cytotoxicity of the selective HDAC6i **9d** in comparison to the unselective HDACi **8c** is in good agreement with recent results from literature, which indicate that class I HDAC inhibition is important for single-agent activity.[51] HDAC6 together with the motor protein dynein is essential to recruit ubiquitinated proteins to aggresomes. The dual inhibition of the aggresome (*via* HDAC6 inhibition) and proteasome pathways can consequently lead to accumulation of misfolded, cytotoxic proteins resulting in induction of apoptosis.[52] Hence, HDAC6i and proteasome inhibitor exhibit synergistic anticancer properties and this synergism led to the approval of the combination therapy of panobinostat, the proteasome inhibitor bortezomib, and dexamethasone to treat multiple myeloma. This knowledge prompted us to investigate the synergistic effects of **8c**, **9d** and vorinostat as a control in combination with bortezomib, using 8 × 8 dose–response matrices (Fig. 5). Among the tested combinations, **8c** displayed the highest synergy (ZIP synergy score: 10.52) with bortezomib, followed by vorinostat (ZIP synergy score: 7.18) and **9d** (5.95). The comparative high synergistic activity of **8c** with bortezomib is potentially due to its potent class I HDAC inhibitory activity, as targeting especially class I HDACs are critical targets to overcome bortezomib resistance.[53]

Conclusions

In summary, we have successfully extended our solid-phase synthesis approach using preloaded resins towards the synthesis of a small compound library of carborane-based HDACis. The syntheses proceeded flawlessly for carborane analogues of benzoic and phenylacetic acid without cluster degradation and intermittent isolation (and detection problems associated with carboranes).[44] These carborane derivatives were employed as bioisosteres in HDACi drug design to precisely steer the selectivity of the HDACis between pan inhibition and highly selective HDAC6 inhibition with only minor adjustments to the inhibitor structure. In reference to the successful FDA-approved HDACi vorinostat, we termed the best-in-category cluster compounds *borinostat A* (**9d**) and *borinostat B* (**8c**). Both borinostats were compared with their respective phenyl analogues **10** and **11** to further support their superiority as a hydrophobic, sterically demanding cap group leading to increased inhibitory activity and, in the case of borinostat A, selectivity for the clinically preferred isoform HDAC6. *In vitro* cytotoxicity evaluation of the new carborane derivatives showed an antiproliferative effect in the low single-digit micromolar range against human ovarian cancer cells and, in the case of borinostat B, submicromolar activity against three different leukemia cell lines. In synergism studies, both borinostat A and B demonstrated synergistic anticancer activity when combined with the proteasome inhibitor bortezomib.

To conclude, due to the tunable selectivity profile, this series of carborane-capped HDACis represents an encouraging starting point to develop unselective HDACis with improved single-agent activity as well as highly selective HDAC6 inhibitors for potential combination therapies.

Author contributions

CS, EH-H, and FKH designed the study. CS performed the synthesis of the carboranes under the supervision of EH-H. CS performed the synthesis of the carborane-capped HDACi under the supervision of FKH. LS provided building blocks and experimental support. AS performed the biochemical HDAC inhibition assays under the supervision of FKH. MH performed the MTT assays under the supervision of FKH. JS-D performed CellTiter Glo assays, western blot experiments and synergy experiments under the supervision of AB and SB. MBS performed the docking studies. CS wrote the manuscript with input from all authors.

Conflicts of interest

There are no conflicts to declare.

Acknowledgements

References

1 (*a*) C. L. Woodcock and R. P. Ghosh, *Cold Spring Harbor Perspect. Biol.*, 2010, **2**, a000596; (*b*) J. R. Whittle and J. Desai, *Cancer*, 2015, **121**, 1164–1167.

2 M. Grunstein, *Nature*, 1997, **389**, 349–352.

3 (*a*) S. Minucci and P. G. Pelicci, *Nat. Rev. Cancer*, 2006, **6**, 38–51; (*b*) M. Haberland, R. L. Montgomery and E. N. Olson, *Nat. Rev. Genet.*, 2009, **10**, 32–42.

4 M. New, H. Olzscha and N. B. La Thangue, *Mol. Oncol.*, 2012, **6**, 637–656.

5 M. Haberland, R. L. Montgomery and E. N. Olson, *Nat. Rev. Genet.*, 2009, **10**, 32–42.

6 Y.-S. Lee, K.-H. Lim, X. Guo, Y. Kawaguchi, Y. Gao, T. Barrientos, P. Ordentlich, X.-F. Wang, C. M. Counter and T.-P. Yao, *Cancer Res.*, 2008, **68**, 7562–7569.

7 T. Sakma, K. Uzawa, T. Onda, M. Shiiba, H. Yokoe, T. Shibahara and H. Tanzawa, *Int. J. Oncol.*, 2006, **29**, 117–124.

8 M. Paris, M. Porcelloni, M. Bnaschi and D. Fattori, *J. Med. Chem.*, 2008, **52**, 1505–1529.

9 N. M. Archin, A. L. Liberty, A. D. Kashuba, S. K. Choudhary, J. D. Kuruc, A. M. Crooks, D. C. Parker, E. M. Anderson, M. F. Kearney, M. C. Strain, D. D. Rochman, M. G. Hudgens, R. J. Bosch, J. M. Coffin, J. J. Eron, D. J. Hazuda and D. M. Margolis, *Nature*, 2012, **487**, 482–485.

10 D. Rotilli, G. Simonetti, A. Savarino, A. T. Palamara, A. R. Migliaccio and A. Mai, *Curr. Top. Med. Chem.*, 2009, **9**, 272–291.

11 S. Trazzi, C. Fuchs, R. Viggiano, M. de Franceschi, E. Valli, P. Jedynak, F. K. Hansen, G. Perini, R. Rimondini, T. Kurz, R. Bartesaghi and E. Ciani, *Hum. Mol. Genet.*, 2016, **25**, 3887–3907.

12 K. J. Falkenberg and R. W. Johnstone, *Nat. Rev. Drug Discovery*, 2014, **13**, 673–691.

13 P. LoPresti, *Cells*, 2021, **10**, 1–15.

14 (a) J. P. Dompierre, J. D. Godin, B. C. Charrin, F. P. Cordelières, S. J. King, S. Humbert and F. Saudou, *J. Neurosci.*, 2007, **27**, 3571–3583; (b) K. J. Falkenberg and R. W. Johnstone, *Nat. Rev. Drug Discovery*, 2014, **13**, 673–691.

15 (a) K. T. Andrews, A. Haque and M. K. Jones, *Immunol. Cell Biol.*, 2012, **90**, 66–77; (b) M. K. W. Mackwitz, E. Hesping, K. Eribez, A. Schöler, Y. Antonova-Koch, J. Held, E. A. Winzeler, K. T. Andrews and F. K. Hansen, *Eur. J. Med. Chem.*, 2021, **211**, 113065; (c) M. K. W. Mackwitz, E. Hesping, Y. Antonova-Koch, S. Diedrich, T. G. Woldearegai, T. Skinner-Adams, M. Clarke, A. Schöler, L. Limbach, T. Kurz, E. A. Winzeler, J. Held, K. T. Andrews and F. K. Hansen, *ChemMedChem*, 2019, **14**, 912–926; (d) D. Diedrich, K. Stenzel, E. Hesping, Y. Antonova-Koch, T. Gebru, S. Duffy, G. Fisher, A. Schöler, S. Meister, T. Kurz, V. M. Avery, E. A. Winzeler, J. Held, K. T. Andrews and F. K. Hansen, *Eur. J. Med. Chem.*, 2018, **158**, 801–813.

16 M. Brindisi, A. P. Saraswati, S. Brogi, S. Gemma, S. Butini and G. Campiani, *J. Med. Chem.*, 2020, **63**, 23–39.

17 B. E. Gryder, Q. H Sodji and A. K. Oyelere, *Future Med. Chem.*, 2012, **4**, 505–524.

18 O. Witt, H. E. Deubzer, T. Milde and I. Oehme, *Cancer Lett.*, 2009, **277**, 8–21.

19 C. Boyault, K. Sadoul, M. Pabion and S. Khochbin, *Oncogene*, 2007, **26**, 5468–5476.

20 (a) C. M. Grozinger and S. L. Schreiber, *Chem. Biol.*, 2002, **9**, 3–16; (b) Y. Li and E. Seto, *Cold Spring Harbor Perspect. Med.*, 2016, **6**, a026831.

21 Y. Sixto-López, J. A. Gómez-Vidal, N. de Pedro, M. Bello, M. C. Rosales-Hernández and J. Correa-Basurto, *Sci. Rep.*, 2020, **10**, 10462.

22 L. Auzzas, A. Larsson, R. Matera, A. Baraldi, B. Deschênes-Simard, G. Giannini, W. Cabri, G. Battistuzzi, G. Gallo, A. Ciacci, L. Vesci, C. Pisano and S. Hanessian, *J. Med. Chem.*, 2010, **53**, 8387–8399.

23 K. V. Butler, J. Kalin, C. Brochier, G. Vistoli, B. Langley and A. P. Kozikowski, *J. Am. Chem. Soc.*, 2010, **132**, 10842–10846.

24 X.-X. Wang, R.-Z. Wan and Z.-P. Liu, *Eur. J. Med. Chem.*, 2018, **143**, 1406–1418.

25 (a) Y. Endo, in *Boron-Based Compounds, Potential and Emerging Applications in Medicine*, ed. E. Hey-Hawkins and C. Viñas Teixidor, John Wiley & Sons Ltd, Oxford, 2018, ch. 1.1.2, pp. 3–5; (b) P. Stockmann, M. Gozzi, R. Kuhnert, M. B. Sárosi and E. Hey-Hawkins, *Chem. Soc. Rev.*, 2019, **48**, 3497–3512.

26 (a) M. Scholz, K. Bensdorf, R. Gust and E. Hey-Hawkins, *ChemMedChem*, 2009, **4**, 746–748; (b) J. F. Valliant, P. Schaffer, K. A. Stephenson and J. F. Britten, *J. Org. Chem.*, 2002, **67**, 383–387.

27 (a) R. N. Grimes, in *Carboranes*, Academic Press, New York, 2nd edn, 2011, pp. 1053–1062; (b) J. F. Valliant, K. J. Guenther, A. S. King, P. Morel, P. Schaffer, O. O. Sogbein and K. A. Stephenson, *Coord. Chem. Rev.*, 2002, **232**, 173–230; (c) R. Frank, V. Ahrens, S. Boehnke, S. Hofmann, M. Kellert, S. Saretz, S. Pandey, M. Sárosi, A. Bartók, A. G. Beck-Sickinger and E. Hey-Hawkins, *Pure Appl. Chem.*, 2015, **87**, 163–171; (d) A. M. Spokoyny, *Pure Appl. Chem.*, 2013, **85**, 903–919; (e) K. O. Kirlikovali, J. C. Axtell, A. Gonzalez, A. C. Phung, S. I. Khan and A. M. Spokoyny, *Chem. Sci.*, 2016, **7**, 5132–5138; (f) G. R. Kracke, M. R. VanGordon, Y. V. Sevryugina, P. J. Kueffer, K. Kabytaev, S. S. Jalisatgi and M. F. Hawthorne, *ChemMedChem*, 2015, **10**, 62–67.

28 For instructive reviews on carboranes, see: (a) V. I. Bregadze, *Chem. Rev.*, 1992, **92**, 209–223; (b) R. E. Williams, *Chem. Rev.*, 1992, **92**, 177–207; (c) R. B. King, *Chem. Rev.*, 2001, **101**, 1119–1152; (d) R. N. Grimes, *Dalton Trans.*, 2015, **44**, 5939–5956.

29 K. Nedunchezhian, N. Aswath, M. Thiruppathy and S. Thirugnanamurthy, *J. Clin. Diagn. Res.*, 2016, **10**, ZE01–ZE04.

30 M. Gozzi, B. Schwarze and E. Hey-Hawkins, *ChemMedChem*, 2021, **16**(10), 1533–1565.

31 M. Otsuka, R. Takita, J. Kanazawa, K. Miyamoto, A. Muranaka and M. Uchiyama, *J. Am. Chem. Soc.*, 2015, **137**, 15082–15085.

32 M. Scholz and E. Hey-Hawkins, *Chem. Rev.*, 2011, **111**(11), 7035–7062.

33 M. Calvaresi and F. Zerbetto, *J. Chem. Inf. Model.*, 2011, **51**, 1882–1896.

34 R. Cheng, B. Li, J. Wu, J. Zhang, Z. Qiu, W. Tang, S.-L. You, Y. Tang and Z. Xie, *J. Am. Chem. Soc.*, 2018, **140**, 4508–4511.

35 D. V. Smil, S. Manku, Y. A. Chantigny, S. Leit, A. Wahhab, T. P. Yan, M. Fournel, C. Maroun, Z. Li, A.-M. Lemieux, A. Nicolescu, J. Rahil, S. Lefebvre, A. Panetta, J. M. Besterman and R. Déziel, *Bioorg. Med. Chem. Lett.*, 2009, **19**, 688–692.

36 N. R. Weinberg, *Curr. Opin. Invest. Drugs*, 2009, **10**, 1236–1242.

37 S. J. Baker, Y.-K. Zhang, T. Akama, A. Lau, H. Zhou, V. Hernandez, W. Mao, M. R. K. Alley, V. Sanders and J. J. Plattner, *J. Med. Chem.*, 2006, **49**, 4447–4450.

38 (a) F. Issa, M. Kassiou and L. M. Rendina, *Chem. Rev.*, 2011, **111**, 5701–5722; (b) M. Bello, *Curr. Pharm. Des.*, 2018, **24**, 1–10; (c) G. F. S. Fernandes, W. A. Denny and J. L. Dos Santos, *Eur. J. Med. Chem.*, 2019, **179**, 791–804.

39 R. Bakri, A. A. Parikesit, C. P. Satriyanto, D. Kerami and U. S. F. Tambunan, *Adv. Bioinf.*, 2014, **2014**, 104823.

40 P. Kavianpour, M. C. M. Gemmell, J. U. Kahlert and L. M. Rendina, *ChemBioChem*, 2020, **21**, 2786–2791.

41 Y. Nie, Y. Wang, J. Miao, Y. Li and Z. Zhang, *J. Organomet. Chem.*, 2015, **798**, 182–188.

42 (*a*) R. A. Wiesboeck and M. F. Hawthorne, *J. Am. Chem. Soc.*, 1964, **86**, 1642–1643; (*b*) M. F. Hawthorne, D. C. Young, P. M. Garrett, D. A. Owen, S. G. Schwerin, F. N. Tebbe and P. A. Wegner, *J. Am. Chem. Soc.*, 1968, **90**, 862–868; (*c*) C. Selg, W. Neumann, P. Lönnecke, E. Hey-Hawkins and K. Zeitler, *Chem.–Eur. J.*, 2017, **23**, 7932.

43 J. Nekvinda, B. Grüner, D. Gabel, W. M. Nau and K. I. Assaf, *Chem.–Eur. J.*, 2018, **24**, 12970–12975.

44 (*a*) T. Lützenburg, I. Neundorf and M. Scholz, *Chem. Phys. Lipids*, 2018, **213**, 62–67; (*b*) M. Scholz and L. M. Wingen, *Inorg. Chem.*, 2017, **56**, 5510–5513.

45 N. Erdeljac, K. Bussmann, A. Schöler, F. K. Hansen and R. Gilmour, *ACS Med. Chem. Lett.*, 2019, **10**, 1336–1340.

46 R. A. Kasar, G. M. Knudsen and S. B. Kahl, *Inorg. Chem.*, 1999, **38**, 2936–2940.

47 L. Sinatra, J. J. Bandolik, M. Roatsch, M. Sönnichsen, C. T. Schoeder, A. Hamacher, A. Schöler, A. Borkhardt, J. Meiler, S. Bhatia, M. U. Kassack and F. K. Hansen, *Angew. Chem., Int. Ed.*, 2020, **59**, 22494–22499.

48 (*a*) Y. Hai and D. W. Christianson, *Nat. Chem. Biol.*, 2016, **12**, 741–747; (*b*) H. M. Berman, J. Westbrook, Z. Feng, G. Gilliland, T. N. Bhat, H. Weissig, I. N. Shindyalov and P. E. Bourne, *Nucleic Acids Res.*, 2000, **28**, 235–242.

49 P. J. Watson, C. J. Millard, A. M. Riley, N. S. Robertson, L. C. Wright, H. Y. Godage, S. M. Cowley, A. G. Jamieson, B. V. Potter and J. W. Schwabe, *Nat. Commun.*, 2016, **7**, 11262.

50 A. Ianevski, L. He, T. Aittokallio and J. Tang, *Bioinformatics*, 2020, **36**, 2645.

51 Y. Depetter, S. Geurs, R. De Vreese, S. Goethals, E. Vandoorn, A. Laevens, J. Steenbrugge, E. Meyer, P. de Tullio, M. Bracke, M. D'hooghe and O. De Wever, *Int. J. Cancer*, 2019, **145**, 735–747.

52 (*a*) T. Hideshima, P. G. Richardson and K. C. Anderson, *Mol. Cancer Ther.*, 2011, **10**, 2034–2042; (*b*) N. Reßing, M. Sönnichsen, J. D. Osko, A. Schöler, J. Schliehe-Diecks, A. Skerhut, A. Borkhardt, J. Hauer, M. U. Kassack, D. W. Christianson, S. Bhatia and F. K. Hansen, *J. Med. Chem.*, 2020, **63**, 10339–10351.

53 J. Kikuchi, T. Wada, R. Shimizu, T. Izumi, M. Akutsu, K. Mitsunaga, K. Noborio-Hatano, M. Nobuyoshi, K. Ozawa, Y. Kano and Y. Furukawa, *Blood*, 2010, **116**, 406–417.

54 S. Shen, M. Svoboda, G. Zhang, M. A. Cavasin, L. Motlova, T. A. McKinsey, J. H. Eubanks, C. Barinka and A. P. Kozikowski, *ACS Med. Chem. Lett.*, 2020, **11**, 706–712.

55 N. J. Porter, A. Mahendran, R. Breslow and D. W. Christianson, *Proc. Natl. Acad. Sci. U. S. A.*, 2017, **114**, 13459.

56 D. Sehnal, A. S. Rose, J. Koča, S. K. Burley and S. Velankar, Mol*: towards a common library and tools for web molecular graphics, in *MolVA'18: Proceedings of the Workshop on Molecular Graphics and Visual Analysis of Molecular Data*, Eurographics Association, Goslar, pp. 29–33.